Dynamic model tracking design for low inertia, high speed permanent magnet ac motors

P. Stewart,* V. Kadirkamanathan

Department of Electronic and Electrical Engineering, University of Sheffield, Mappin Street, Sheffield S1 3JD, United Kingdom

Abstract

Permanent magnet ac (PMAC) motors have existed in various configurations for many years. The advent of rare-earth magnets and their associated highly elevated levels of magnetic flux makes the permanent magnet motor attractive for many high performance applications from computer disk drives to all electric racing cars. The use of batteries as a prime storage element carries a cost penalty in terms of the unladen weight of the vehicle. Minimizing this cost function requires the minimum electric motor size and weight to be specified, while still retaining acceptable levels of output torque. This tradeoff can be achieved by applying a technique known as flux weakening which will be investigated in this paper. The technique allows the speed range of a PMAC motor to be greatly increased, giving a constant power range of more than 4:1. A dynamic model reference controller is presented which has advantages in ease of implementation, and is particularly suited to dynamic low inertia applications such as clutchless gear changing in high performance electric vehicles. The benefits of this approach are to maximize the torque speed envelope of the motor, particularly advantageous when considering low inertia operation. The controller is examined experimentally, confirming the predicted performance.

Keywords: Permanent magnet ac motor; Model reference; flux weakening

1. Introduction

Permanent magnet motors fed by pulse width modulated (PWM) inverters have historically been used for a wide variety of industrial applications, in particular servo drives [1,2]. This preference is due to the inherent high power density and low rotor inertia of the motor. These advantages have outweighed the added complexity of electronic commutation of the motor. Permanent magnet machines fall into two distinct classes, namely sinusoidally excited, and trapezoidally excited. The inverter topology most widely used to excite both types of permanent magnet machine is the three phase full bridge inverter. The standard semiconductor switch in use in three phase inverters is the insulated gate bipolar transistor (IGBT), the gate switching sequence being responsible for the shaping of current waveforms appropriate for each type of machine. A voltage sourced configuration is more popular than the current sourced configuration due to factors such as cost, weight, and dynamic response. The addition of closed-loop current control yields a configuration referred to as current-regulated voltage-sourced inverter. The closed-loop system behaves like a current-sourced inverter with an extremely fast dynamic response time. This configuration depends on the internal motor phase inductances combined with closed-loop control to provide current-sourced characteristics without the need for an external inductor.

*Tel: +44 (0)114 2225841. *E-mail address*: p.stewart@sheffield.ac.uk

While some applications require only torque control, many others require position and velocity control which in the simplest case is achieved by successively closing outer servo loops around a central current controller. Proportional and integral error amplifiers are generally sufficient for closing the position and velocity loops [3–5], however, a variety of sophisticated adaptive control algorithms have also been developed [6–8].

The major control problem when considering both steady-state and dynamic operation of the permanent magnetic ac (PMAC) motor can be seen to be the finite voltage and current supply available from the dc link and the inverter. The PMAC motor will be analyzed in a reference frame which is obtained via a nonlinear transform. It will be shown that as the machine's rotor accelerates, the rising value of back emf restricts the magnitude of torque producing current until further torque production is not possible. The general PMAC motor is analyzed in a manner which makes possible a controller which effectively increases the useful speed range of the motor, and in particular takes account of the voltage drop due to the current dynamics.

2. PMAC motor analysis

$d-q$ analysis which has historically been applied to induction motors has been found to be an ideal tool both in terms of describing the PMAC machine and designing control methods. The method has the advantages of simplicity and an associated graphical description which facilitates understanding of the operating processes of the machine. The analysis is a steady-state method, and as such provides a dc description of an ac machine via a nonlinear transform. The $d-q$ analysis of the motor has found further support since the industry standard form of mapping the performance of a newly designed motor is to characterize its torque speed map in terms of rotor velocity, torque output, and angle of current vector advance [9] (see Fig. 1). The torque speed map is then transferred onto a DSP in the form of a vector look-up table, to perform torque control. The experimental data contained in the look-up table represents a steady-state $d-q$ description of the motor, which provides values to be tracked by d and q axis proportional and integral (PI) current controllers.

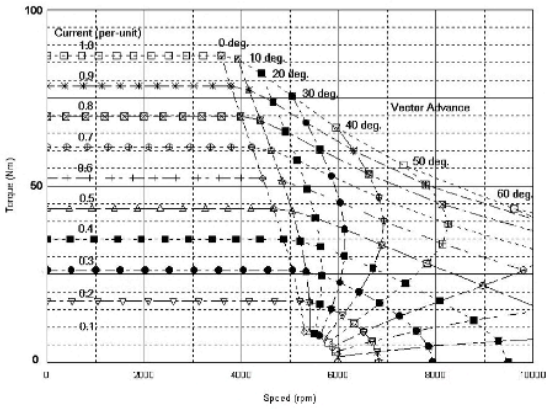

Fig. 1. Experimental torque, speed, current vector advance map.

As magnet technology and materials allowed higher flux densities to be produced, particularly with the advent of rare-earth permanent magnets (e.g., Ne-Fe-B), the power densities obtained from the new generation of PMAC motors led to its introduction as vehicle traction drives for electric vehicles. Traction drives and industrial spindle drives require the motor to be able to operate in the constant power region. The principal features of the operation are: the constant torque region of operation where the applied voltage is larger than the back emf, base speed which is the critical point where the applied voltage equals the back emf voltage, and finally the constant power region where the back emf voltage is larger than the applied voltage. Again the $d-q$ analysis of the motor allows control to be performed in the constant power or flux weakening region. The principal characteristics of the permanent magnet ac synchronous motor are that the distribution of magnet flux in the motor airgap is sinusoidal or quasisinusoidal, the applied current waveforms are sinusoidal or quasisinusoidal, and the stator conductors have a quasisinusoidal distribution. The class of PMAC motors under consideration here are termed "surface mount" due to the permanent magnets being mounted on the surface of the rotor. A rotor with surface mounted magnets (Fig. 2) exhibits little or no saliency with the d-axis and q-axis inductances being almost identical. This contrasts with a rotor with inset magnets (Fig. 3) which exhibits saliency since the d-axis inductance is less than the q-axis inductance. The sinu-

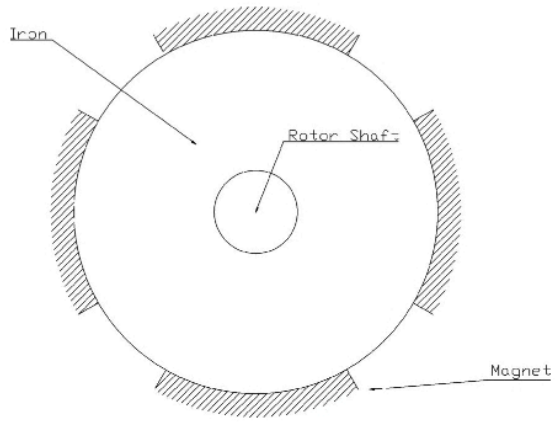

Fig. 2. Smooth rotor with surface mounted magnets.

soidal magnet-flux distribution around the airgap is achieved by tapering the magnet thickness at the pole edges, and typically using a magnet pole arc of 120°. A current regulated pulse width modulated (PWM) inverter is used to achieve the best approximation of sinusoidal current waveforms [10].

3. The $d-q$ nonlinear transformation

The $d-q$ model of the PMAC is applied to facilitate the application of high performance control techniques. This description of the motor has evolved from steady-state analysis of wound rotor synchronous machines and involves the transformation of three phase alternating current and voltage quantities into an orthogonal reference frame containing current and voltage vectors. The stator currents are transformed into an orthogonal frame of reference which is moving synchronously with the rotor flux. The orthogonal reference frame is derived from the phase currents via the Park transform [11–13], to give

$$V_q = r\, i_q + \omega\, L\, i_d + \omega\, \kappa + L\left(\frac{di_q}{dt}\right), \qquad (1)$$

$$V_d = r\, i_d - \omega\, L\, i_q + L\left(\frac{di_d}{dt}\right), \qquad (2)$$

where V_d, V_q are the d and q axis voltages, i_d, i_q are the d and q axis currents, r is the phase resistance, ω is the rotor velocity, L the phase inductance and κ the back emf constant in the reference frame as volts/radians/second. The q-axis inductance is equivalent to the armature inductance, and the d-axis inductance is equivalent to the field inductance in a field wound dc motor. In the case of the smooth rotor PMAC motor, these quantities are equal. The d and q variables are obtained from the three phase quantities via the following definition of the Park transform,

$$\begin{bmatrix} V_q \\ V_d \end{bmatrix} = \frac{2}{3}\begin{bmatrix} \cos(\theta) & \cos\left(\theta - \frac{2\pi}{3}\right) & \cos\left(\theta + \frac{2\pi}{3}\right) \\ \sin(\theta) & \sin\left(\theta - \frac{2\pi}{3}\right) & \sin\left(\theta + \frac{2\pi}{3}\right) \end{bmatrix} \times \begin{bmatrix} V_a \\ V_b \\ V_c \end{bmatrix}, \qquad (3)$$

where $V_{a,b,c}$ are the three phase elements. This transformation also applies to current and flux linkage quantities, and the three phase quantities may be obtained from the d and q axis variables by application of an inversion of the Park matrix in Eq. (3). Fast responding current regulation combined with self-synchronization by incorporating a shaft encoder make it possible to orientate the instantaneous current phasor I anywhere within the $d-q$ reference frame subject to supply current and voltage constraints. The speed of the torque response is dependent on the source voltage and stator inductance values. The torque ripple generated by sinusoidal PMAC machines is generally less than trapezoidal machines, providing one of

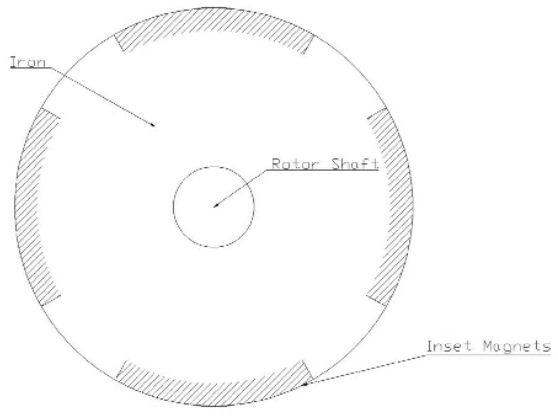

Fig. 3. Salient rotor with inset magnets.

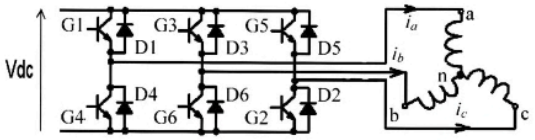

Fig. 4. Three phase full bridge inverter for a permanent magnet motor drive.

the principal motivations for their current popularity in high performance applications. Although secondary sources of torque ripple exist (winding harmonics etc.), standard techniques are available to attenuate them [14]. Sinusoidal PMAC machines can thus be designed to exhibit extremely low ($<3\%$) torque ripple, excluding the high-frequency PWM components which are effectively filtered out by the combined motor and load inertia. The inverter topology most widely used for excitement of sinusoidal permanent magnet machines is the three phase full-bridge inverter (Fig. 4). Switch gating sequences ($G1-G6$) for the six insulated gate bipolar transistors (IGBT's) are responsible for the conversion of the dc supply voltage (Vdc) into sinusoidal phase excitation waveforms, in addition to adjusting amplitudes and frequency. Flyback diodes ($D1-D6$) provide energy paths during four quadrant operation of the machine [15]. The three phase currents are generated by pulsewidth modulated (PWM) current regulators ([11]). The three stator currents are measured by transducers and compared to the reference currents producing error signals which are fed forward via PI controllers to comparators which compare the error signals to sawtooth triangular waveforms.

If the current error signal is larger than the sawtooth, the voltage is switched positively, while if the current error signal is smaller than the sawtooth, the voltage is switched negatively. Thus the depth of PWM modulation defines the positive and negative on-time ratio.

High-speed operation of the PMAC machine is constrained by the linear proportionality of the back emf and inductive voltage drops to rotor velocity. The current regulators naturally saturate to six-step excitation with 180° switch conduction intervals in this mode of operation, since depth of modulation for all three phases is 100%. In order to operate above base speed, the current phasor trajectory must move into the second quadrant of the $d-q$ complex plane, which corresponds to an advance of the current vector angle. This allows current and thus torque to be produced at higher speeds, even though the torque per amp values are lower than those obtained along the q axis. The torque speed envelope is expanded in this case to a ratio greater than 4:1, following a constant power hyperbola ($T_e\omega_m = P_o$) in the high-speed region. This technique is known as flux weakening since negative d axis stator flux ($L_d i_d$) is being added to counteract the positive d-axis magnet emf κ. The limiting torque-speed envelope that can be achieved with a given PMAC machine under optimum flux-weakening conditions is determined by the machine's electrical parameters [16]. The system operates subject to the constraints (4) on voltage and current,

$$V_s^2 \geqslant V_q^2 + V_d^2, \quad I^2 \geqslant i_q^2 + i_d^2, \tag{4}$$

where V_s is the magnitude of the voltage vector and I is the magnitude of the current vector. The amount of current that can be supplied by the three phase inverter is limited by the heat dissipation properties of the motor, and by the current rating of the inverter. It is also limited by the converter dc link voltage, which must overcome both the emf, and the voltage drops across the synchronous reactance and resistance. Considering the system constraints, maximum torque-per-amp operation below base speed requires the d-axis current to be controlled to zero. Above this boundary, the rising emf value can be countered by advancing the current vector with respect to the rotor (field or flux weakening), and introducing negative d-axis current. The requirements of the flux-weakening controller are to calculate the velocity at which flux weakening is to be initiated, and to output optimal d-axis and q-axis current commands in steady-state and dynamic operation. The most convenient description of the system is the steady-state circle diagram, in the $d-q$ reference frame. If resistance is neglected, then from Eqs. (1) and (2) the steady-state system becomes Eqs. (5) and (6), and the instantaneous torque T_e for the surface mount PMAC motor is given by Eq. (7), where k_t is the motor torque constant,

$$V_q = \omega L i_d + \omega \kappa, \tag{5}$$

$$V_d = -\omega L i_q, \tag{6}$$

$$T_e = k_t i_q. \tag{7}$$

In the current phasor complex plane, the current limit is defined by a circular locus defined by the constraints in expression (4). Similarly, the maximum available inverter voltage limits the current vector to a circular locus with frequency-dependent radius, and different center $(-\kappa/L,0)$, where κ is the back emf constant. The voltage limit locus is derived from the identity in constraint expression (4), then in steady state,

$$V^2=\omega^2 L^2 i_q^2+(\omega \kappa+\omega L i_d)^2, \tag{8}$$

and

$$\frac{V}{\omega L}=\sqrt{i_q^2+\left(i_d+\frac{\kappa}{L}\right)^2}. \tag{9}$$

As speed and frequency increase, the current limit locus remains fixed, however, the radius of the voltage limit locus decreases. Eventually the PWM control saturates when its duty cycle reaches maximum, and the available sine-wave voltage from the inverter equals the phase voltage. This operating point is known as ''base speed'' and occurs at the intersection of the q axis, current limit circle, and voltage limit circle. If the rotor velocity increases further, the radius of the voltage limit circle decreases further, and maximum current is defined by a current vector terminating in the intersection of the two circles. As rotor velocity increases, the voltage limit circle drags the current phasor further and further ahead of the q axis, decreasing the torque producing current, and increasing the demagnetizing negative d axis current. This acceleration can increase until the point where the current vector lies entirely in the demagnetizing direction, and no further torque production is possible.

4. Flux weakening methods

The flux weakening algorithms can be separated into two distinct approaches. In all cases below base speed, the current vector is controlled to lie along the q axis for the smooth-rotor-type motor. Above base speed, the amount of torque producing current and current vector advance is either directly calculated by means of the system equations, or a mechanism exists to converge upon the optimal current trajectory via feedback of transformed current errors. Taking first the automatic algorithms, on entering the flux weakening region, the current vector initially lies outside the limit circle imposed by the applied voltage limit and the growing magnitude of the generated emf. Based on the existence of current errors in the orthogonal frame, the current vector is forced to converge to some point on the limit circle by the action of the feedback error gains [17,13]. A major advantage claimed for this type of controller is that it does not rely on motor parameters to calculate the necessary control action, and that unmodeled voltage drops and model inaccuracies are automatically accounted for within the control action. The method does have a number of drawbacks. The method relies on the onset of current regulator saturation to drive the flux weakening algorithm. When current regulator saturation occurs, however, the PWM regulation is at a modulation depth of 100%, and no further dc link voltage is available to achieve dynamic control of the current vector. With reference to the voltage equations for the motor in the orthogonal reference frame,

$$V_d=ri_d-\omega L i_q+L\frac{di_d}{dt}, \tag{10}$$

$$V_q=ri_q+\omega(Li_d+\kappa)+L\frac{di_q}{dt}, \tag{11}$$

since $V_d^2+V_q^2$ is bounded by V^2, no voltage is available to drive the derivative terms at the present level of torque. In order to converge to an optimal current vector position, the q-axis demand must be depressed and negative d-axis current injected. The response to error will be a function of the controller gains and the motor electrical time constants with the result that even if optimal gain values are selected, a finite amount of time will be required for the controller to converge to an acceptable solution. Most importantly, while the controller will eventually converge to a point on the voltage limit ellipse, no mechanism exists to guarantee that the convergence point is on the maximum torque per amp trajectory. Although the method does not rely directly upon the system parameters, the feedback error gains must be ascertained either by simulation or experimentation. In effect, the knowledge of the motor parameters is substituted by parameter-dependent gain values which must be experimentally defined. No analysis has been presented to prove the robustness of the system against parameter variations in concert with the speed and accuracy of the convergence to

a solution. Examining the methods which calculate the d-axis and q-axis commands directly [18–21], the convergence problem has been overcome based on knowledge of the machine parameters such as phase inductance and dc link voltage, calculations give i_d^* and i_q^*. The automatic controllers have been designed in an attempt to avoid the modeling errors introduced by this reliance on parameter knowledge. However, dc link voltage can be directly measured, and although the motor parameters are slowly time varying due to temperature effects, the initial manufactured motor parameters are accurately known, and the application of parameter estimation techniques in real time should enable the controller to operate effectively. The direct calculation technique gives an instantaneous command set based on the present motor operating conditions with no time lag or degradation due to convergence and so should give superior performance when compared to other techniques. In Ref. [22], this type of approach is shown to be very effective. In the application under consideration here, with extremely low inertias, it has been found that the approach adopted in Ref. [22] can be extended to include the current dynamics, and thus increase the performance of the motor. The preferred type of technique is thus structured as a model reference controller with inputs rotor velocity and torque demand, and outputs i_d^* and i_q^* which are the current demand values. The outputs act as demands to orthogonal controllers which force the motor currents to track the command values.

5. Model reference controller

The operating principle of model reference control systems is to specify system performance, using a model which gives the desired output for a given input. The form of the model can be hardware (i.e., the output of an op-amp.) or software (i.e., a mathematical model of the desired plant response). The controller compares the output of the model with that of the process, and the control signals are generated as a function of the difference between plant and process. Thus, in the case of the PMAC motor, a model reference will be derived from the analytic solution of the system equation under the constraint of minimum current vector magnitude at all times. The output of the model provides reference values for the $d-q$ components of the current vector. Rearranging the system Eq. (1) gives the reference model

$$i_q^* = V_q^* - \omega L i_d^* - \omega \kappa \tag{12}$$

and by substituting Eqs. (12) and (2) into the supply voltage constrained voltage vector,

$$V = \sqrt{V_q^{*2} + V_d^{*2}}, \tag{13}$$

and the expression for instantaneous torque,

$$T_e^* = \frac{3P}{2} \phi_f i_q^* = k_t i_q^*, \tag{14}$$

yields an expression which describes the torque producing component of the system in terms of the physical parameters, torque constant k_t, and speed variable ω;

$$T_e^* = \frac{k_t}{\omega L} \sqrt{V^2 - \omega^2 \kappa^2} = k_t \sqrt{\left(\frac{V}{\omega L}\right)^2 - \left(\frac{\kappa}{L}\right)^2}, \tag{15}$$

also

$$V^2 = (\omega L i_d^* + \omega \kappa)^2 - (\omega L i_q^*)^2. \tag{16}$$

Combining Eqs. (15) and (16) yields

$$\left(\frac{V}{\omega L}\right)^2 = \left(i_d^{*2} + \frac{\kappa}{L}\right)^2 + \left(\frac{T_e^*}{k_t}\right)^2, \tag{17}$$

which describes the frequency-dependent voltage vector in terms of the current components, and forms the model for calculating the system command outputs for the PMAC drive operating modes. The steady-state representation for control purposes found in other methods is unsatisfactory due to its exclusion of the dynamic components of the system equations. The dynamic system Eqs. (10) and (11) represent the balance between the supply voltage components and the system operational voltage drops. Other minor voltage drops and dynamics exist such as the semiconductor voltage drops in the power electronic inverter, and freewheeling current flow in the flyback diodes, but are omitted here for the sake of clarity. The omission of the current dynamics has the fundamental consequence that the components which represent the advance of the current vector with respect to time are unmodeled, and consequently a maximum voltage drop of magnitude

$$\Delta V = \sqrt{\left(L\frac{di_d}{dt}\right)^2 + \left(L\frac{di_q}{dt}\right)^2} \qquad (18)$$

has been ignored. Thus when the PMAC enters the field weakening region and the current regulators saturate, no spare voltage is available to acommodate the dynamic movement of the current vector, and consequently the optimal path for the maximum torque profile cannot be followed.

5.1. Modeling the dynamic voltage drop

An equation can be derived to describe the rate of change of the angle of the current vector in the $d-q$ reference frame. Ignoring resistive effects, we obtain an expression in the steady state which relates the supply voltage to the rotor velocity,

$$V^2 = \omega^2 L^2 i_q^2 + (\omega\kappa + \omega L i_d)^2. \qquad (19)$$

The aim of the method presented here is to obtain expressions which describe the motion through which the current vector angle advances in the flux weakening region, and which can be used to extend the model reference controller to include the dynamic terms. This control extension will be designed to reserve sufficient voltage headroom by dynamic allocation in the field weakening region, avoiding the torque-speed envelope degradation experienced with the steady-state model reference controller. This expression in Eq. (19) is differentiated and solved for $d\sigma/dt$ where σ is the angle of current vector advance ahead of the q axis. In order to obtain a description of the current vector dynamics, using

$$\frac{d\omega}{dt} = \frac{T}{J} = \frac{k_t I\cos\sigma}{J} \qquad (20)$$

we obtain an expression for the current vector advance angle which allows calculation from the system parameters and measured current, assuming that the limits I and V are treated as constants;

$$\frac{d\sigma}{dt} = \frac{-k_t(L^2I^2 + 2LI\sin(\sigma)\kappa + \kappa^2)}{\omega\kappa LJ}, \qquad (21)$$

which shows the dependence on the system inertia. The derivatives of the $d-q$ currents are given by

$$\left(\frac{di_q}{dt}\right) = -i_d\left(\frac{d\sigma}{dt}\right), \qquad (22)$$

$$\left(\frac{di_d}{dt}\right) = i_q\left(\frac{d\sigma}{dt}\right) \qquad (23)$$

and obtain the voltage drop due to the current vector angle dynamics,

$$\Delta V = \frac{-k_t LI(L^2I^2 + 2L_sI\sin(\sigma)\kappa + \kappa^2)}{\omega\kappa L_s J}, \qquad (24)$$

where δV is the dynamic voltage drop.

5.2. Dynamic base speed

Whichever method of controller is applied to achieve field weakening, this voltage drop either explicitly or implicitly must be included in order to achieve the highest possible torque speed profile. Also, although the corner frequency calculated for steady-state operation is still valid, under dynamic conditions, the onset of flux weakening will occur at a lower frequency than in the steady state due to the voltage necessary to drive the current vector phase dynamics. At this new virtual base speed, which represents the boundary between the constant torque and constant power regions, the d-axis current is set to zero, and the equation for dynamic voltage drop reduces to

$$\Delta V = \frac{ILk_t(L^2I^2 + \kappa^2)}{\omega\kappa J}. \qquad (25)$$

An expression can be derived from the circle diagram description to link the difference between the magnitudes of the voltage-frequency limit circles at dynamic and steady-state base speeds, where V_s is the magnitude of the applied voltage,

$$\Delta V = V_s - \sqrt{I^2 + \omega L\frac{\kappa^2}{L^2}}, \qquad (26)$$

combining Eqs. (25) and (26) gives a quadratic expression which relates the rotor velocity to a dynamic base speed which is dependent on the applied current variable,

$$0 = -\omega^2 L\sqrt{I^2 + \frac{\kappa^2}{L^2}} + V_s\omega - \frac{ILk_t(L^2I^2 + \kappa^2)}{\kappa J}. \qquad (27)$$

The solution of this equation gives the difference between the steady-state base speed ω_o (calculated at the intersection between the current limit circle,

the voltage limit circle and the q-axis current axis), and the dynamic base speed ω_d where

$$\omega_d = \omega_o - \Delta\omega \tag{28}$$

and

$$\Delta\omega = \omega_o\left(\frac{V_s k_t I L_s}{\kappa J \omega_s^2}\right). \tag{29}$$

The performance of the model reference controller can be enhanced by including the effects of the dynamic terms, and also the voltage drop due to the resistive parameters which are present as an unmodeled effect. The approach used will be to reserve voltage headroom to allow the current vector to follow its optimal path, and also reserve voltage headroom to reflect the unmodeled voltage drop due to resistive effects. Expressions have been derived to describe both the voltage drop due to dynamic effects which is given as Eq. (24) and also the dynamic base speed associated with this dynamic effect which is given as Eq. (27). Now in the steady-state model reference controller, the current vector I is calculated as extending from (0,0) in the $d-q$ frame to the intersection of the current limit circle and the frequency related voltage limit circle with radius $V/\omega L$ and center $(-\kappa/L,0)$. The outputs of the reference model are the commanded q-axis current i_q^* and the commanded d-axis current i_d^* (which are changing as the motor accelerates). In order to reserve sufficient voltage headroom to allow the current dynamics to act effectively, the length of the voltage limit vector $V/\omega L$ must be reduced by an appropriate amount. The voltage reserved for this effect has d-axis and q-axis components and can be described as being a vector extending from the voltage limit vector in the reference model. The d-axis and q-axis current commands are now formulated as the intersection of the dynamic voltage drop (which augments the steady-state voltage limit vector) and the current limit circle. For the benefit of reduced computation in the model reference controller, the voltage drop due to the dynamics can be approximated as a worst case. That is the magnitude of the dynamic voltage drop is calculated and subtracted from the magnitude of the voltage limit vector, the new voltage limit vector including the dynamic components being represented as V_l,

$$V_l = V_s - \Delta V. \tag{30}$$

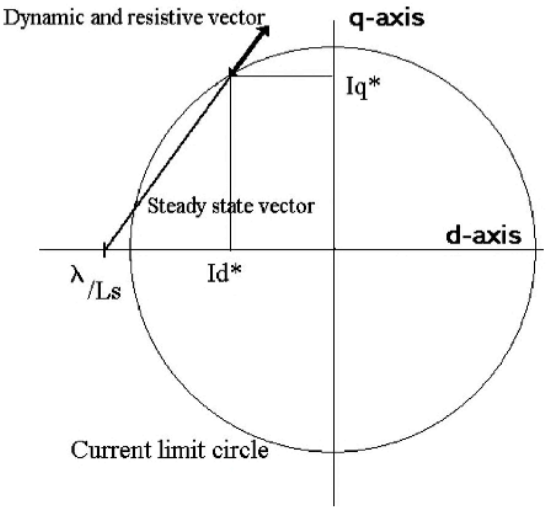

Fig. 5. PMAC dynamic model reference control geometric implementation.

Similarly, the unmodeled voltage drop due to resistive effects can be included as a worst case effect, and thus the voltage limit vector now contains all the significant system voltage drops, with any minor unmodeled drops being lumped together in the worst case adoption of vector directions. The voltage limit vector now becomes

$$V_l = \frac{\kappa}{\omega L} - \Delta V - rI. \tag{31}$$

If this voltage can be reserved in operation, coupled with a revised base speed to enable the reservation process, then the machine should follow the optimal current trajectory with current regulators held just within the bounds of saturation. The geometric implementation in the model reference controller is shown in Fig. 5. The calculations involved in the implementation of this algorithm are relatively straightforward. The steady-state model reference which has already been implemented is utilized. In steady-state form, the reference model is supplied by a set of memory registers which contain the parameters neccessary to calculate the circle diagram representation with voltage and current limit vectors. The parameters such as inductance and emf constant are known or measurable values. The value for dc link supply voltage is measured directly from the dc supply which is either a battery or Ward-Leonard dc generator. The magnitude of the dynamic voltage drop

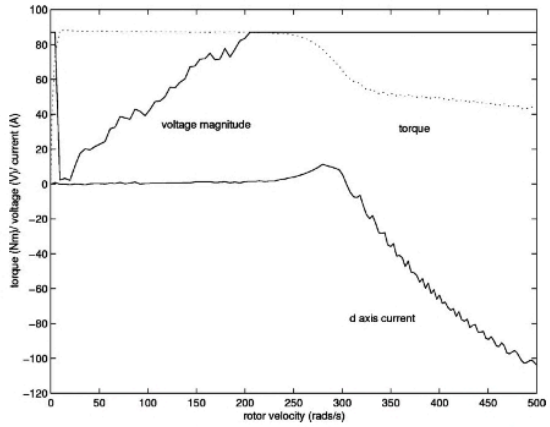

Fig. 6. Field weakening controller, dynamic operation, drive motor inertia only. Comparison of d-axis current, supply voltage magnitude, and produced torque.

is calculated using Eq. (31), which is supplied to the steady-state model reference controller. This revised dc link value is appropriate to the steady-state description, with the correct value of voltage reserved to allow dynamic operation, with the unmodeled resistive voltage drop now included. The model reference outputs command values as before and is unaware that voltage has been reserved for dynamic operation. The final part of the implementation is the calculation and use of the revised base speed. An expression has been derived to calculate the new dynamic base speed in Eq. (28). This value is used to switch the voltage reservation algorithm in and out. Below dynamic base speed, the dynamic voltage drop is not subtracted, subtraction only taking place above this new base speed.

6. Extending the controller to include current dynamics

A survey of all the proposed flux weakening schemes in the literature demonstrate the same fundamental weakness. As previously described, the key to all the flux weakening control algorithms is to identify the onset of current regulator saturation, detection feedback being provided by the buildup of error between the commanded and actual d-axis current. If we examine Fig. 6 which is a simulation of the system freely accelerating under maximum torque command and no external inertial load with a typical flux weakening controller described in Ref. [17], it is possible to identify the typical shortcomings of existing control strategies. No information is given in any of the literature to calculate the proportional or integral gains for any of the PI controllers present in the controllers to execute the automatic field weakening. These controller parameters are critical to supressing the q-axis current demand and command negative d-axis current. In order to perform this simulation, the gains were tuned "on the fly" to achieve the best possible torque speed envelope. We find that the current regulators saturate (i.e., the voltage magnitude reaches a maximum) and torque production begins to tail off before any d-axis current error is present. Error is detected by the existing methods such as in Refs. [17,23], etc., when the d-axis current goes positive [24]. This scheme will result in a suboptimal torque-speed trajectory, its difference from the optimal path being a function of the system inertia. This simulation describes the worst case, since the motor is driving only its own rotor inertia. In terms of actual operation, this reduced envelope can be ignored if ultimate performance is not the objective of the controller. The degradation will also be a function of how well the gains of the controller have been chosen and tuned, and the overall inertia being accelerated. If the motor application specification requires the maximum torque speed profile to be the highest possible for the given dc link voltage and motor current limit, or if it is necessary to perform servo operations on just the rotor inertia, then a controller must be developed which provides the maximum torque profile even in the low inertia servo case. In the case of the traction drive with a clutchless gearbox, the rotor velocity must be reduced by 50% and then track the output shaft velocity at minimum torque output to achieve gearchanging. This deceleration is a function of the maximum torque envelope and requires a controller to be designed which overcomes the problem of accurately controlling the current vector in the face of current controller saturation.

7. Experimental results

The model reference controller with the dynamic extension reserving voltage headroom were implemented on a TI TMS320C5 digital signal processing (DSP) board, controlling a 45-kW, per-

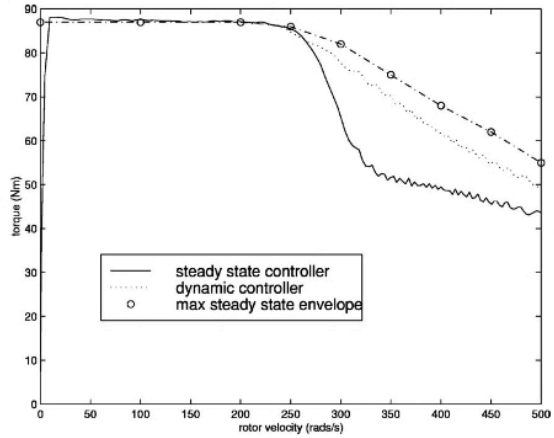

Fig. 7. Performance comparisons of the reference model controller with and without the dynamic extension. Rotor only inertial load.

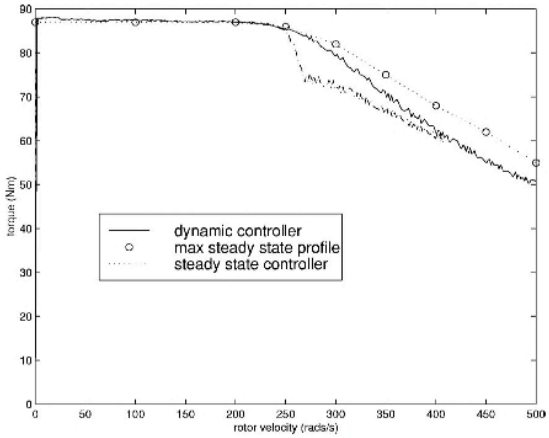

Fig. 8. Performance comparisons of the model reference controller with and without the dynamic extension. Rotor and external load motor inertial load.

manent magnet ac motor producing a peak torque of 87 Nm, and mounted on a four quadrant dynamometer. The 16-bit DSP was mounted on a proprietary evaluation board which allowed convenient access to interface the current, position and voltage measurement devices to its onboard analogue to digital converters. A three-phase PWM with programmable carrier frequency set at 10 kHz output was available from the DSP and fed directly into a three-phase four-quadrant inverter. Due to the dynamic bandwidth limitations of torque transducers, the instantaneous torque is calculated from the q-axis current. The first experiment is for the motor with just the rotor inertia and no external load. This is the most severe test due to rotor acceleration, and should show the greatest deterioration in torque output. The rotor is allowed to accelerate freely from rest under maximum torque demand in order to compare with the maximum torque envelope. The relative performance can be seen in Fig. 7. The optimal torque speed envelope is obtained by operating the motor at steady-state points, and ascertaining the maximum torque output on a dynamometer. This is labeled on the graph as *max steady state envelope*. This is a set of discrete torque measurements taken at a range of speeds when all transients have decayed to zero, and represents the maximum torque which can be produced by the system at any speed. The series labeled *steady state controller* represents the maximum torque envelope produced by a machine operating dynamically with model reference being produced by the steady state representation. Finally, the series labeled *dynamic controller* is the maximum torque envelope of the motor freely accelerating, and being controlled by the model reference augmented by the dynamic voltage reservation scheme. The experiment shows that the dynamic controller has produced a greatly enhanced torque envelope when compared to the controller based on the steady-state system description. The difference in maximum torque at any point between the dynamic controller and the max steady-state envelope is due to the fact that under steady-state conditions, no voltage is required for the current vector dynamics, and consequently more voltage is available for torque production. The experiment of the motor driving an external load giving a combined inertia of $J = 0.41$ kgm was repeated with the dynamic controller. The comparison of the maximum torque envelope of this simulation is shown in Fig. 8. This maximum torque envelope is compared with the steady-state controller operating dynamically with the same inertia and also the maximum steady-state torque profile. The divergence between the performance of the dynamic and steady-state model reference controllers is now markedly less pronounced as predicted. The torque profiles of the two regimes converge around 400 rad s^{-1} as the unmodeled dynamic voltage drop experienced by the steady state controller begins to diminish. Examination of Fig. 9 reveals the predicted action of the dynamic and steady-state

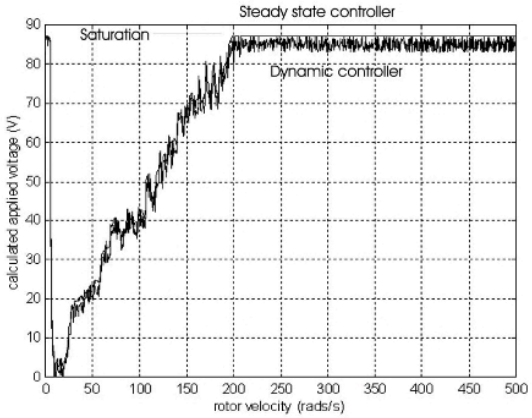

Fig. 9. Applied voltage magnitude, comparison of dynamic and steady state controller.

controllers. At the boundary with the field weakening region, the steady-state current controllers saturate, and the applied voltage is subject to a PWM modulation depth of 100%. The dynamic controller operates just within the saturation limit, and thus maintains control of the current vector at all times throughout the operating range of the motor. The simulations confirm the requirement of extending the model reference controller with the dynamic voltage reservation scheme. The improvement in performance when the motor is driving a relatively light load is particularly pronounced. Considering Fig. 7 for the rotor only inertial load, a peak advantage for the dynamic control scheme of 18 Nm is gained at 360 rad s^{-1} tailing to 7 Nm at the peak operating velocity of 500 rad s^{-1}. In the case of the traction application under study here, much of the dynamic operation takes place around base speed, and the enhanced torque profile made available by the dynamic scheme allows the fastest possible gear changes. This enhancement would also be important for low inertia servo applications. With reference to the current regulators saturating during high speed operation, Fig. 9 illustrates the operation of the dynamic controller with respect to the performance of the steady state derived controller. A saturation level of 87 V relates to the maximum voltage available from the dc supply. The steady-state controller saturates at around 200 rad s^{-1} and consequently loses accurate current control since only six step excitation is available above this operating point. This corresponds to the drop in torque production displayed in Figs. 7 and 8. The dynamic controller, however, holds the magnitude of the applied voltage vector just below the level of saturation, and hence retains full control of the current vector. This results in the elevated levels of torque above base speed for the dynamic controller which are illustrated in Figs. 7 and 8.

8. Conclusion

A controller has been designed, simulated, and experimentally investigated, which maximizes the torque speed envelope of the PMAC motor. It has the advantages of relatively simple implementation, and in practice requires no tuning for any arbitary motor. The gains for the tracking controller were found via a Monte Carlo search of all the PI parameter combinations within a practical search space. An objective criteria was formulated to rank the potential solutions during the iterative process. The objective function sought to minimize current rise time, overshoot, steady-state error, and settling time in response to a step current demand input. The search algorithm was terminated when a response with a damping factor between 0.7 and 0.71 was identified. These PI parameters which were chosen by this procedure correlated closely with gains which had been found via simulation tuning, and in practice are simply found by increasing the proportional gain to achieve good dynamic performance, and increasing the integral gain to achieve good tracking. All this compares favorably with other proposed schemes which require tuning of the field weakening controller gains for each individual motor. The approach is found to have particular benefits for maximizing the torque envelope with low inertia applications, where the effects of the dynamic voltage drop are the most pronounced, due to the fast acceleration of the rotor. As shown in Fig. 10, the controller with the dynamic extensions is able to achieve faster transition times due to the elevated torque envelope which has been made available. This has been found to be of particular benefit in (for example) clutchless gear changing on electric vehicles, where the concept of ‘‘driveability’’ indicates that lags which are only of the order of milliseconds can influence the driver’s perception of the vehicle’s performance. The application of the dynamic extension can contribute to the increase in this perception of ‘‘drive-

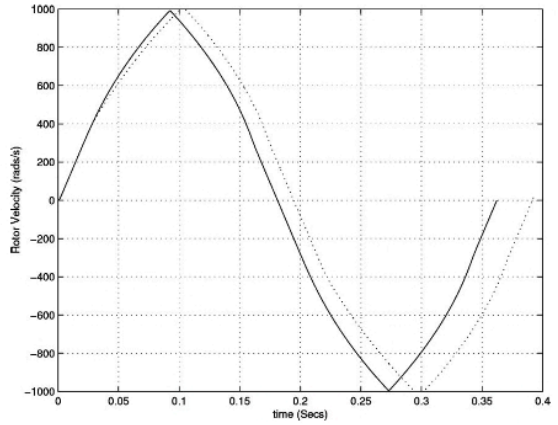

Fig. 10. Test velocity profile, comparison of dynamic and steady-state based controller.

ability'' due to the increase in available torque envelope in the flux weakening region resulting in faster gear change transitions, and is thus a useful implementation.

References

[1] Hopkins, M. N., DC Motors, Speed Controls and Servo Systems, 1st ed. Electrocraft Corp., Gallipolis, 1972.

[2] Slemon, G. R. and Gumaste, A. V., Steady-state analysis of a PM synchronous motor drive with current source inverters. IEEE Trans. Ind. Appl. **1A**, 190–197 (1983).

[3] Astrom, K. J. and Hagglund, T., The future of PID control. IFAC workshop on digital control, PID2000, pp. 19–30, 5–7 April 2000, Terrassa, Spain.

[4] Tan, K. K., Wang, Q. C., and Hagglund, T., Advances in Industrial Control. Springer-Verlag, Berlin, 1999.

[5] Zhuang, M. and Atherton, D. P., Tuning of optimum PID controllers. Proc. IEEE **140**, 216–224 (1993).

[6] Yamamoto, T., Fujii, K., and Kaneda, M., A design of self-tuning PID controllers based on a pole assignment scheme. 14th World Congress of IFAC, pp. 259–264, Beijing, China, 1999.

[7] Moden, P. E., Experiences with adaptive control since 1982. Proceedings of the 34th IEEE conference on decision and control, pp. 667–672, New Orleans, Louisiana, 1995.

[8] Bengtsson, G. and Egardt, B., Experiences with self-tuning control in the process industry. Proceedings of the 9th IFAC World Congress, pp. 32–140, Budapest, Hungary, 1984.

[9] Jahns, T. M., Torque production in permanent magnet synchronous motor drives with rectangular current excitation. IEEE Trans. Ind. Appl. **20**, 803–813 (1984).

[10] Miller, T. J. E., Brushless permanent magnet and reluctance motor drives. Oxford University Press, Oxford, 1993.

[11] Pillay, P. and Krishnan, R., Modelling, simulation, and analysis of permanent magnet motor drives, part 1: The permanent magnet synchronous motor drive. IEEE Trans. Ind. Appl. **25**, 265–273 (1989).

[12] Hindmarsh, J., Electrical Machines and Drives. Pergamon Press, Oxford, U.K., 1985.

[13] Kim, J. M. and Sul, S. K., Speed control of interior permanent magnet synchronous motor drive for the flux-weakening operation. IEEE Trans. Ind. Appl. **33**, 43–48 (1997).

[14] Slemon, G. R. and Straughen, A., Electric machines. Addison-Wesley, Reading, MA (1980).

[15] Jahns, T. M., Motion control with permanent-magnet AC machines. Proc. IEEE **82**, 1241–1252 (1994).

[16] Schiferl, R. and Lipo, T. A., Power capability of salient pole PM synchronous motors in variable speed drive applications. IEEE Trans. Ind. Appl. **26**, 115–123 (1990).

[17] Sudhoff, S. D., Corzine, K. A., and Hegner, H. J., A flux weakening strategy for current regulated surface mounted permanent magnet machine drives. IEEE Trans. Energy Convers. **10**, 431–437 (1995).

[18] Morimoto, S., Takeda, Y., Hirasa, T., and Taniguchi, K., Expansion of operating limits for permanent magnet motor by current vector control considering inverter capacity. IEEE Trans. Ind. Appl. **26**, 866–871 (1990).

[19] Dhouadi, R. and Mohan, N., Analysis of current regulated voltage-source inverters for permanent magnet synchronous motor drives in normal and extended speed ranges. IEEE Trans. Energy Convers. **15**, 137–144 (1990).

[20] Macminn, S. R. and Jahns, T. M., Control techniques for improved high speed performance of interior permanent magnet synchronous motor drives. IEEE Trans. Ind. Appl. **27**, 997–1004 (1991).

[21] Morimoto, S. and Takeda, Y., Wide speed operation of interior permanent magnet synchronous motors with high performance current regulator. IEEE Trans. Ind. Appl. **30**, 920–926 (1994).

[22] Verl, A. and Bodson, M., Torque maximisation for permanent magnet synchronous motors. IEEE Trans. Control Syst. Technol. **6**, 740–744 (1998).

[23] Hirasa, T. and Takeda, Y., Current phase control methods for permanent magnet synchronous motors considering saliency. PESC Conference Recordings, pp. 409–414, April 1988.

[24] Jahns, T. M., Flux weakening regime operation of an interior permanent magnet synchronous motor drive. IEEE Trans. Ind. Appl. **1A-23**, 681–689 (1987).